

Non-Invasive Hemodynamic Assessment of Aortic Coarctation: Validation with *In Vivo* Measurements

LUCIAN ITU,^{1,2} PUNEET SHARMA,¹ KRISTÓF RALOVICH,^{1,3} VIOREL MIHALEF,¹ RAZVAN IONASEC,¹
ALLEN EVERETT,⁴ RICHARD RINGEL,⁴ ALI KAMEN,¹ and DORIN COMANICIU¹

¹Siemens Corporate Research and Technology, 755 College Road East, Princeton, NJ 08540, USA; ²Transilvania University of Brasov, Str. Politehnicii nr. 1, Brasov 500024, Romania; ³Technical University of Munich, Boltzmannstr. 3, Garching 85748, Germany; and ⁴Pediatric Cardiology, Johns Hopkins University School of Medicine, 600 N. Wolfe Street, Baltimore, MD 21287, USA

(Received 28 August 2012; accepted 27 November 2012; published online 12 December 2012)

Associate Editor Scott L. Diamond oversaw the review of this article.

Abstract—We propose a CFD-based approach for the non-invasive hemodynamic assessment of pre- and post-operative coarctation of aorta (CoA) patients. Under our approach, the pressure gradient across the coarctation is determined from computational modeling based on physiological principles, medical imaging data, and routine non-invasive clinical measurements. The main constituents of our approach are a reduced-order model for computing blood flow in patient-specific aortic geometries, a parameter estimation procedure for determining patient-specific boundary conditions and vessel wall parameters from non-invasive measurements, and a comprehensive pressure-drop formulation coupled with the overall reduced-order model. The proposed CFD-based algorithm is fully automatic, requiring no iterative tuning procedures for matching the computed results to observed patient data, and requires approximately 6–8 min of computation time on a standard personal computer (Intel Core2 Duo CPU, 3.06 GHz), thus making it feasible for use in a clinical setting. The initial validation studies for the pressure-drop computations have been performed on four patient datasets with native or recurrent coarctation, by comparing the results with the invasively measured peak pressure gradients recorded during routine cardiac catheterization procedure. The preliminary results are promising, with a mean absolute error of less than 2 mmHg in all the patients.

Keywords—Pressure gradient, CFD, Reduced-order models, Coarctation of aorta, Non-invasive, PC-MRI.

NOMENCLATURE

c Wave speed
 C Windkessel compliance

DBP/SBP Diastolic/systolic blood pressure
 E Young's modulus
 HR Heart rate
 K_v/K_t
 K_u/K_c Viscous/turbulent/inertance/continuous pressure-drop coefficient
 L_c Coarctation length
MAP Mean arterial pressure
 Q_{asc}/Q_{desc} Flow rate through the ascending/descending aorta
 Q_{CoA} Flow rate through the coarctation
 $Q_{supra-aortic}$ Flow rate through supra-aortic vessels
 R_c Coarctation resistance
 $R_d/R_p/R_t$ Distal/proximal/total Windkessel resistance
 Z Characteristic impedance

INTRODUCTION

Coarctation of the aorta (CoA) is a congenital cardiac defect usually consisting of a discrete shelf-like narrowing of the aortic media into the lumen of the aorta, occurring in 5 to 8% of all patients with congenital heart disease.¹⁸ Patients born with CoA require lifelong medical/surgical care, which includes invasive and non-invasive imaging, drug therapy, and, if the CoA recurs, invasive catheterization or surgical intervention to reduce the blood pressure in the ascending aorta. For pre-operative evaluation of CoA severity and post-operative assessment of residual narrowing, a number of techniques are used in clinical settings. Anatomical assessment is usually based on Magnetic Resonance Imaging (MRI) or Computed Tomography

Address correspondence to Lucian Itu, Siemens Corporate Research and Technology, 755 College Road East, Princeton, NJ 08540, USA. Electronic mail: lucian.itu@unitbv.ro

(CT), while the functional assessment is performed by measuring the pressure gradient (ΔP) across the coarctation. The most accurate assessment of the trans-coarctation pressure gradient is by invasive catheter based measurements during cardiac catheterization. Other less accurate alternatives include blood pressure measurements in upper and lower body extremities (arms and legs) and taking the difference, estimating peak/mean gradients from Doppler echocardiography, or estimation from Phase-Contrast MRI (PC-MRI) based on 2-D or 3-D flow measurements.

Measurements derived from Doppler echocardiography are often not obtainable in the older child and adult due to the posterior location of the descending aorta and have been reported to overestimate the pressure gradient, both with the simplified and the modified Bernoulli's equation.²⁰ In other studies, the difference between the blood pressures in the arms and legs has been shown to be an unreliable estimate for the pressure gradient through the coarctation,⁶ when compared to the clinical gold-standard obtained by invasive cardiac catheterization to measure the peak-to-peak ΔP across the coarctation. Given the invasive nature of cardiac catheterization, and the patient's exposure to radiation and contrast agent, an accurate non-invasive assessment of pressure gradients would not only eliminate these drawbacks, but also help lower the overall costs for both pre- and post-operative assessment of CoA.

To address this issue, Computational Fluid Dynamics (CFD) based models have been proposed in recent years, for analyzing the hemodynamics in idealized and/or patient-specific healthy and diseased aortic geometries. These studies have analyzed the pressure-drop along the coarctation using rigid²³ or compliant vessel walls,¹¹ oscillatory wall shear stress²⁶ and turbulence intensity.¹ There has also been work to assess the mechanical alterations introduced by coarctation and their impact on vascular structure in rabbits.¹² The increased focus on *in vivo* validation of such approaches is the first step towards transitioning them into clinical decision making. To make CFD-based methods feasible in a clinical setting, the second major hurdle is to ensure that they fit in a clinical workflow. Solution of the 3-D Navier–Stokes equations in complex patient-specific geometries usually requires several hours for data preparation, meshing and numerical computation time, which severely limits their scope in a routine clinical setting.

To address these challenges, we present a CFD-based approach coupled with a novel, non-invasive model personalization strategy for the assessment of pre- and post-intervention CoA patients. The key features of our approach are—(i) reduced-order model

for computing blood flow in patient-specific aortic geometries, (ii) a parameter estimation approach for determining patient-specific boundary conditions and vessel wall parameters from non-invasive measurements, and (iii) a comprehensive pressure-drop formulation. Our approach is fully automatic, requiring no iterative tuning procedures, and a total of 6–8 min for the computation (on Intel Core2 Duo CPU, 3.06 GHz), being thus feasible in a clinical setting. The initial validation for the trans-coarctation computations has been performed on four patient datasets against the clinical gold-standard, by comparing the results with the invasively acquired measurements during cardiac catheterization. Additionally, we have also compared the results with two non-invasive surrogate measures often used in clinical practice, namely the Doppler-derived pressure-gradient from modified Bernoulli's equation and the cuff-pressure derived gradient obtained from the difference of the blood pressure in the upper and lower body extremities.

MATERIALS AND METHODS

For a feasible approach to accurately compute pressure-drop in clinical settings, the total execution time of the algorithm is paramount. Keeping this in mind, we have chosen a quasi 1-D approach, which, together with the terminal Windkessel elements, represents a reduced-order blood flow model for the aorta. The reduced-order approach is at least two orders of magnitude faster than most 3-D flow computations, while being able to accurately predict time-varying pressure and flow rate values for patient-specific models.¹⁷ As a next step towards performing patient-specific flow computations, we have developed a parameter estimation procedure for 'personalizing' the model parameters by using non-invasively measured clinical measurements from the patient, an approach which we have previously introduced in a preliminary form.¹⁵ The estimation is done in conjunction with a comprehensive pressure-drop model which is coupled with the reduced-order flow model to estimate the pressure-drop for an individual patient.

For our method, we use a time-varying flow rate waveform at the inlet (derived from 2-D PC-MRI data) and three-element Windkessel elements at each outlet (brachiocephalic, left common carotid, left subclavian and descending aorta). The approach can be used for both pre- and post-operative data. In the following we focus though on the pre-operative case, since it is the more challenging one and it is clinically more significant. Figure 1 displays an overview of the approach for the pre-operative case.

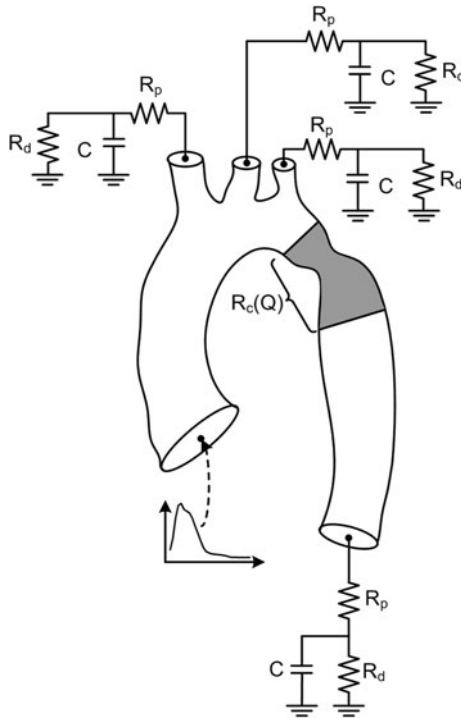


FIGURE 1. Overview of the pre-operative modeling approach: time-varying flow rate is imposed at the inlet and three-element Windkessel models are coupled at the outlets; a flow-dependent resistance is introduced in order to account for the pressure drop along the coarctation.

Reduced-Order Model for Blood Flow Computation

The proximal vessels are modeled as axi-symmetric 1-D vessel segments, where the flow satisfies the following properties: conservation of mass, conservation of momentum, and a state equation for wall deformation (Eqs. 1–3). The vessel wall is modeled as a purely elastic material.

$$\frac{\partial A(x, t)}{\partial t} + \frac{\partial q(x, t)}{\partial x} = 0, \quad (1)$$

$$\begin{aligned} \frac{\partial q(x, t)}{\partial t} + \frac{\partial}{\partial t} \left(\alpha \frac{q^2(x, t)}{A(x, t)} \right) + \frac{A(x, t)}{\rho} \frac{\partial p(x, t)}{\partial x} \\ = K_R \frac{q(x, t)}{A(x, t)}, \end{aligned} \quad (2)$$

$$p(x, t) = \frac{4 Eh}{3 r_0} \left(1 - \sqrt{\frac{A_0}{A(x, t)}} \right) + p_0, \quad (3)$$

where α is the momentum-flux correction coefficient, K_R is a friction parameter, E is the Young modulus, h is the wall thickness and r_0 is the initial radius corresponding to the pressure p_0 .

One of the assumptions made during the derivation of the reduced-order model is that the axial velocity is dominant and the radial components are negligible.

This assumption holds well for normal, healthy vessels, but in case of sudden changes in lumen diameter, e.g., for a narrowing like the coarctation, the radial components can no longer be excluded. Thus, we introduced a pressure-drop model (described in the next section) for the coarctation segment to account for the resistance introduced by the coarctation. For the implementation, we coupled this segment with the proximal and distal segments of the aorta by enforcing continuity of total pressure and flow.

At each bifurcation we enforce the continuity of flow and total pressure as follows:

$$q_p = \sum_i (q_d)_i, \quad (4)$$

$$p_p + \frac{1}{2} \rho \frac{q_p^2}{A_p^2} = (p_d)_i + \frac{1}{2} \rho \frac{(q_d)_i^2}{(A_d)_i^2}, \quad (5)$$

where subscript p refers to the parent, while d refers to the daughter vessels of the bifurcation.

At the outlets, the Windkessel equation is applied in order to close the system of equations:

$$\frac{\partial p}{\partial t} = R_p \frac{\partial q}{\partial t} - \frac{p}{R_d \cdot C} + \frac{q(R_p + R_d)}{R_d \cdot C}, \quad (6)$$

The inlet boundary condition is prescribed by the time-varying flow rate determined through PC-MRI, while the estimation of the wall properties and the Windkessel parameters at the outlets are described in the following sections. We performed the numerical computations using the explicit, finite difference, second-order Lax-Wendroff method. The system of non-linear equations obtained at the junctions was solved iteratively using the Newton–Raphson method.

Parameter Estimation for Model Personalization

Patient-specific blood flow computations require physiologically appropriate boundary conditions at the inlet and the outlet of the computational domain. Depending on the availability of *in vivo* measurements and the underlying assumptions of the model, researchers typically use one of the following inlet boundary condition: (i) time-varying velocity (or flow rate) profile,^{11,14} or (ii) a lumped model of the heart coupled at the inlet.^{3,4} The former can be easily determined in a clinical setting, and is often part of the diagnostic workflow (2-D/3-D Phase-contrast MRI, Doppler ultrasound). These measurements can be mapped to the computational domain at the inlet using plug, parabolic or Womersley profile. The alternate approach is to couple a lumped model of the upstream circulation (e.g., a lumped model of the heart) and adjust the model parameters to obtain physiological

flows and pressures in the computational domain. For the outlet boundary condition, physiologically motivated three-element Windkessel boundary conditions are used widely.^{22,24} This requires estimation of three quantities (two resistances: proximal— R_p , and distal— R_d , and one compliance— C) at each outlet from non-invasive data.

The main constituents of the personalization framework are the estimation of inlet and outlet conditions, coupling a pressure-drop model, and an estimation of the mechanical properties of the aortic wall from the acquired patient data.

Estimation of Boundary Conditions and Pressure-Drop Model

Mean arterial pressure (MAP), defined as the average pressure over the cardiac cycle is responsible for driving the blood into the distal vessels and ultimately in the tissues. MAP is related to the total distal resistance by the following expression:

$$\text{MAP} = Q \cdot R.$$

where Q is the average flow at a point in the arterial circulation, and R is the total distal arterial resistance. For the aorta, the following equation holds at each outlet i :

$$\text{MAP} = Q_i \cdot (R_t)_i, \quad (7)$$

where Q_i is the average flow rate through outlet i and $(R_t)_i$ is the total resistance, which is the sum of the two Windkessel resistances ($R_t = R_p + R_d$). In the ascending aorta, MAP is estimated from the non-invasive cuff pressures,¹⁶ as given below:

$$\text{MAP} = \text{DBP} + \left[\frac{1}{3} + (\text{HR} \cdot 0.0012) \right] \cdot (\text{SBP} - \text{DBP}), \quad (8)$$

where HR is the heart rate and SBP (DBP) are the systolic (diastolic) blood pressures.

The time-averaged flow rates at the ascending (Q_{asc}) and at the descending aorta (Q_{desc}) are measured from the PC-MRI slices. Thus the total flow to the three supra-aortic outlet vessels ($Q_{\text{supra-aortic}}$) is determined by $Q_{\text{supra-aortic}} = Q_{\text{asc}} - Q_{\text{desc}}$.

For the first few branches starting from the aortic root, the flow is distributed to the branching vessels proportionally to the square of the radius.²⁸ Thus,

$$Q_i = Q_{\text{supra-aortic}} \cdot r_i^2 / \sum_{i=1}^3 r_i^2, \quad (9)$$

where r_i is the radius of the supra-aortic branch i . Since the pressure difference between the ascending aorta and the three supra-aortic branches is insignificant (the

viscous losses are negligible), the same average pressure is used to estimate the total resistance.

$$(R_t)_i = \frac{\text{MAP}}{Q_i}. \quad (10)$$

For the CoA patients, the above assumption does not hold true for the descending aorta because the narrowing at the coarctation site introduces a pressure-drop along the length of the aorta, which can be translated into a flow-dependent resistance $R_c(Q)$. Thus, the total resistance, which represents the sum of the resistance of the coarctation and that of the outlet Windkessel model, is estimated as follows:

$$(R_t)_{\text{desc}} + R_c(Q) = \frac{\text{MAP}}{Q_{\text{desc}}}. \quad (11)$$

The flow-dependent resistance is estimated based on a pressure-drop model. Table 1 displays various pressure-drop models which were previously introduced in the literature. Based on these, we propose the following comprehensive pressure-drop model for the coarctation:

$$\begin{aligned} \Delta P = & K_v(\alpha) \cdot R_{vc}q + \frac{\rho K_t}{2A_0^2} \left(\frac{A_0}{A_c} - 1 \right)^2 |q|q \\ & + K_u L_u \frac{\partial q}{\partial t} + K_c(\alpha) R_{vc}\bar{q}, \end{aligned} \quad (12)$$

where the first term captures the viscous losses, the second term captures the turbulent losses, the third term represents the inertial effect and the fourth term is a continuous component. $K_v = 1 + 0.053 \cdot (A_c/A_0)\alpha^2$ is a viscosity coefficient and $R_{vc} = \frac{8\mu}{\pi} \int_0^{L_c} \frac{1}{r^4(l)} dl$ is the viscous resistance; $K_t = 1.52$ is a turbulence coefficient; $K_u = 1.2$ is an inertance coefficient and $L_u = \frac{\rho}{\pi} \int_0^{L_c} \frac{1}{r^2(l)} dl$ is the inertance; $K_c = 0.0018\alpha^2$ is a continuous coefficient, α being the Womersley number. The start and end cross-sections of the coarctation were taken as the locations where the radius decreases under 95% of the reference value for the corresponding location, and respectively increases above 95% of the reference value for the corresponding location. The specific formulations of the viscous and the inertial term used in Eq. (12) were chosen because of their ability to take into account the shape of the coarctation. This allows us to personalize the pressure-drop model for a patient-specific geometry of the coarctation. The turbulent term has been successfully used in different, independent studies performed *in vitro*¹⁹ and *in vivo*.²¹ We also included a continuous term, which has been introduced previously² as a result of the phase difference between the flow rate and the pressure drop identified in a computational study.

TABLE 1. Pressure-drop models.

Model	Equation	Quantities
Model 1 ²⁷	$\Delta P = \frac{\mu K_c}{2\pi r_0^3} q + \frac{\mu K_c}{2A_0} \left(\frac{A_0}{A_c} - 1 \right)^2 q q + \frac{\mu K_c L_c}{A_0} \frac{\partial q}{\partial t}$	A_0 —normal cross-sectional area; A_c —coarctation minimum cross-sectional area; L_c —coarctation length; $K_v = \frac{16L_c}{r_0} \left(\frac{A_0}{A_c} \right)^2$, $L_a = 0.83 \cdot L_c + 3.28 \cdot r_c$, $K_f = 1.52$, $K_u = 1.2$
Model 2 ²²	$\Delta P = K_v(x) \cdot R_{vc} q + \frac{\mu K_c}{2A_0} \left(\frac{A_0}{A_c} - 1 \right)^2 q q + K_u L_u \frac{\partial q}{\partial t} + K_c(x) R_{vc} \bar{q}$	$K_v = 1 + 0.053 \frac{A_0}{A_c} x^2$ $K_f = 0.95$, $K_u = 1.2$, $K_c = 0.0018 x^2$ $\alpha = r_0 \sqrt{\frac{2\pi r_0^3}{\mu}}$, where f —frequency $R_{vc} = \frac{8\mu}{\pi} \int_0^{L_c} \frac{1}{r^3(l)} dl$, $L_u = \frac{L_c}{\pi} \int_0^{L_c} \frac{1}{r^2(l)} dl$
Model 3 ⁵	$\Delta P = \frac{\mu q^2}{2} \left(\frac{1}{A_c} - \frac{1}{A_0} \right)^2 + \frac{\mu a}{\sqrt{A_0}} \left(\frac{A_0}{A_c} - 1 \right) \frac{\partial q}{\partial t}$	$a = 2\pi$ —empirically determined parameter; $b = 0.5$ —empirically determined parameter.

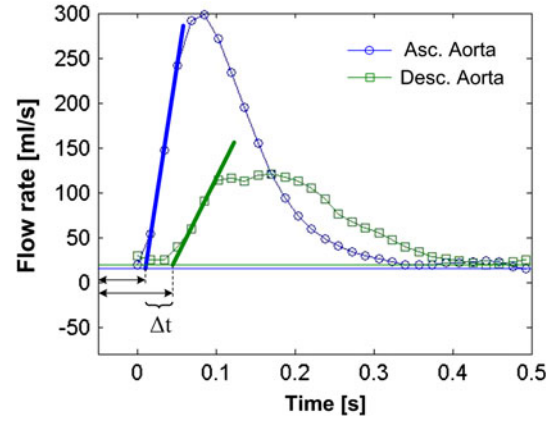


FIGURE 2. Estimation of the flow transit time between ascending aorta (blue circles) and the descending aorta (green squares). The upslope curve is approximated by the line connecting the points lying at 20 and 80% of the maximum flow rate. The time Δt is determined by the interval between the onset (the intersection point of the upslope curve and the minimum flow rate) of the two flow curves.

Since the model contains both a linear and a square term of the flow rate, we investigate two different approaches for the evaluation of the resistance introduced by the coarctation:

Approach 1: the resistance is computed using the average flow rate at the descending aorta:

$$R_{c1}(Q) = \Delta P(\bar{Q}_{desc}) / \bar{Q}_{desc}; \quad (13)$$

Approach 2: the resistance is computed by averaging the resistances of each time frame:

$$R_{c2}(Q) = \left(\sum_1^n \Delta P(q_{desc}(t)) / q_{desc}(t) \right) / n, \quad (14)$$

whereas $\Delta P(\cdot)$ is computed through Eq. (12), and n is the number of frames acquired through PC-MRI.

The proximal resistance at each outlet point is equal to the characteristic resistance of the vessel (in order to minimize the reflections), which is computed as follows:

$$(R_p)_i = \frac{1}{\pi \cdot r_i^2} \sqrt{\frac{2 \cdot \rho \cdot E \cdot h}{3 \cdot r_i}}, \quad (15)$$

where $E \cdot h / r_i$ is estimated as described later. Next, the distal resistance is computed by subtracting the proximal resistance from the total resistance.

For the estimation of compliance values, we first compute the total compliance²² (C_{tot}). Next, the compliance of the proximal vessels (C_{prox}) is computed by summing up the volume compliances of each proximal segment. Thus,

$$(C_{prox})_j = \int \frac{3 \cdot A}{2} \cdot \frac{r_j}{E \cdot h} dl, \quad (16)$$

where A is the cross-sectional area. Finally, the total outlet compliance (C_{out}) is determined by subtracting C_{prox} from C_{tot} , which is then distributed to the four outlets as follows:

$$(C_{\text{out}})_i = \frac{C_{\text{out}} \cdot r_i^2}{\sum_{i=1}^3 r_i^2}. \quad (17)$$

Estimation of Aortic Wall Parameters

An important aspect of a blood flow computation with compliant walls is the estimation of the mechanical properties of the aortic wall. We use a method based on wave-speed computation,¹⁴ where the wave-speed is related to the properties of the aortic wall by the following expression:

$$c = \sqrt{\frac{2}{3 \cdot \rho} \cdot \frac{E \cdot h}{r_0}}, \quad (18)$$

where c is the wave speed. To estimate the wave speed, we use the transit-time method,⁷ whereby $c = \Delta x / \Delta t$.

Here Δx is the distance (measured along the centerline) between the inflow at the aortic root and the outlet at the descending aorta, and Δt is the time taken by the flow waveform to travel from the inlet to the outlet location. The time Δt is determined by the interval between the onset (foot) of the two flow curves. The location of the onset (foot) is determined by the intersection point of the upslope curve and the minimum flow rate (Fig. 2). The upslope curve is approximated by the line connecting the points at 20 and 80% of the maximum flow rate at the particular location.

Once the wave speed is computed, the quantity $E \cdot h / r_0$, in Eqs. (15), (16), and (18), is computed as:

$$\frac{E \cdot h}{r_0} = \frac{3 \cdot \rho \cdot c^2}{2}. \quad (19)$$

The wall properties of all the aortic segments are determined using this equation. To estimate the wall properties of the supra-aortic vessels, we use a slightly modified approach, under which the wall properties of each supra-aortic segment are computed separately. This is done to minimize the wave reflections at the bifurcations. Under this approach, first the reflection coefficient at a bifurcation is computed¹³:

$$\Gamma = \frac{Y_p - \sum_i (Y_d)_i}{Y_p + \sum_i (Y_d)_i}. \quad (20)$$

where Y_p (Y_d) is the characteristic admittance of the parent (daughter) vessel. The characteristic admittance is the inverse of the characteristic resistance of a vessel [computed as in Eq. (15)]. There are three bifurcations, one for each supra-aortic vessel, and the characteristic resistance of each supra-aortic vessel is computed by setting Γ equal to 0:

$$R_{\text{supra-aortic}} = R_{\text{aorta-p}} \cdot R_{\text{aorta-d}} / (R_{\text{aorta-p}} - R_{\text{aorta-d}}) \quad (21)$$

Once the characteristic resistance is known, $E \cdot h / r_0$, is determined as follows [from Eq. (4)]:

$$\frac{E \cdot h}{r_0} = \frac{3 \cdot Z_{\text{supra-aortic}} \cdot \pi^2 \cdot r_0^4}{2 \cdot \rho}. \quad (22)$$

To avoid non-physiological wave speeds in the supra-aortic vessels, a minimum threshold of 200 cm/s and a maximum threshold of 1200 cm/s are imposed in each supra-aortic vessel.

Figure 3 summarizes the estimation methodology described in the last two subsections, while Table 2 lists all input parameters which are required, together with their source. For the post-operative case, if a residual narrowing is identifiable, then the same procedure can be applied.

RESULTS

We validated our methodology by investigating 5 random COAST patient datasets with native and/or recurrent coarctation which involved the aortic isthmus or the first segment of the descending aorta. The patients' clinical data originated from the FDA approved, multi-center COAST trial.¹⁸ Important for our investigation, COAST mandates recording mean values of catheter based blood pressure measurements in different locations (ascending aorta—AAo, transverse aortic arch—TAA, and descending aorta—DAo) at systolic and diastolic phases over multiple heart cycles. Further, the study includes the following imaging data: 3-D contrast enhanced MR angiograms (MRA) and flow sensitive 2-D CINE phase contrast MR (PC-MR) images. Angiograms depict the thorax including the TAA and supra aortic arteries and enable accurate segmentation of the lumen of the vessel tree. The segmented 3-D geometric model of the vessel tree was used to calculate the artery centerlines and various radii measurements. The PC-MR images (typically oblique axial time-series encoding through-plane velocities) intersect the aorta twice. Once in the region of the aortic root and, second the DAo below the isthmus/coarctation. The different images were readily registered based on MR machine coordinates, after

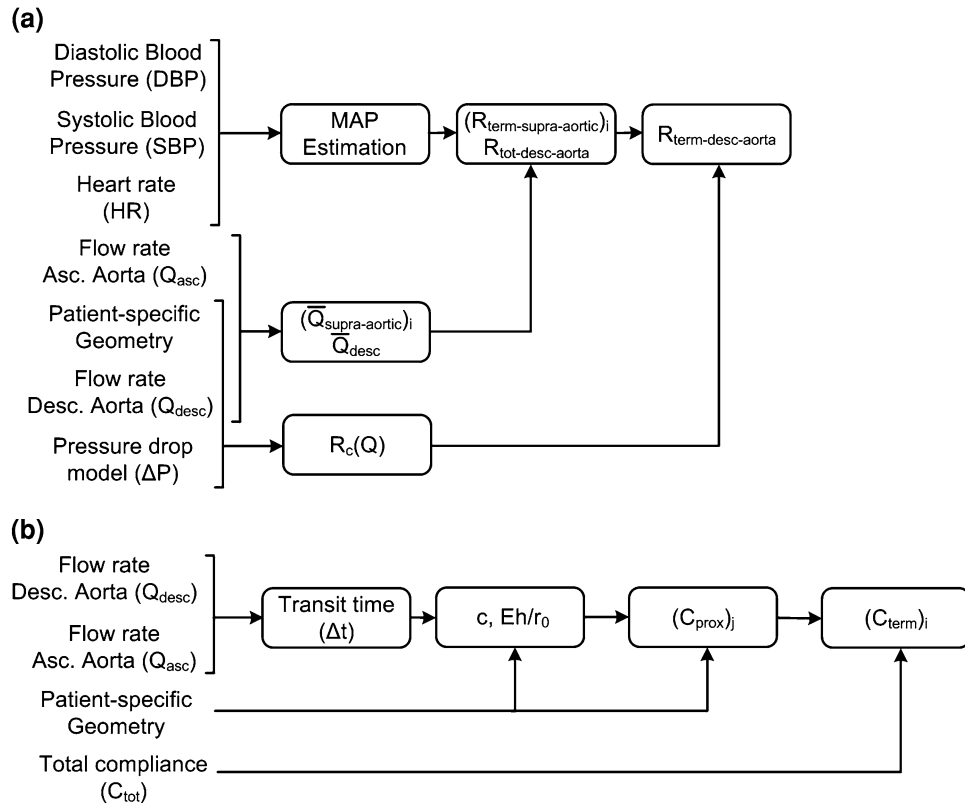


FIGURE 3. Non-invasive personalization strategy for (a) terminal Windkessel resistances, and (b) terminal Windkessel compliances and wall properties. Non-invasively acquired input parameters are specified on the left.

TABLE 2. List of input parameters.

Input	Source
Systolic blood pressure (SBP)	Cuff measurement (arms)
Diastolic blood pressure (DBP)	Cuff measurement (arms)
Heart rate (<i>HR</i>)	Routine measurement
Flow rate asc. aorta (<i>Q_{asc}</i>)	2-D PC-MRI
Flow rate desc. aorta (<i>Q_{desc}</i>)	2-D PC-MRI
Patient-specific geometry	Magnetic Resonance Angiography (MRA)
Pressure-drop model (ΔP)	Fluid dynamics theory, <i>in vitro</i> experiments
Total compliance (<i>C_{tot}</i>)	Clinical literature

registration, the PC-MR images were segmented and integrated to derive personalized inflow and outflow profiles. The overall pre-processing pipeline is illustrated in Fig. 4. The details of the image segmentation and other geometric pre-processing steps were reported previously,²⁵ together with a validation study with clinical evaluation.

To build the discretized geometric mesh from the centerline and cross-sectional areas, we used an approach similar to previously introduced ones,²¹ wherein for each vessel of the arterial model, we used several distinct 1-D segments with spatially varying cross-sectional area values in order to obtain a geometry close to the 3-D geometry acquired through MRI. The solution at the interface locations between the

separate 1-D segments was determined by considering continuity of flow rate and total pressure, similarly to bifurcation solutions [Eqs. (4) and (5)].

After reviewing MR images for patient 5, we observed an incorrect PC plane location (intersecting AV and LVOT instead of AAO) that resulted in an erroneous inflow. Thus, only 4 patients were included in the final evaluation procedure, which is described in the following.

Table 3 displays the patient-specific data. Three sets of cuff-pressure measurements were performed in the arms and legs, and the average values were used to compute the difference between the upper body (arms) and lower body (legs) pressures at systole and diastole. Doppler echocardiography measurements of peak

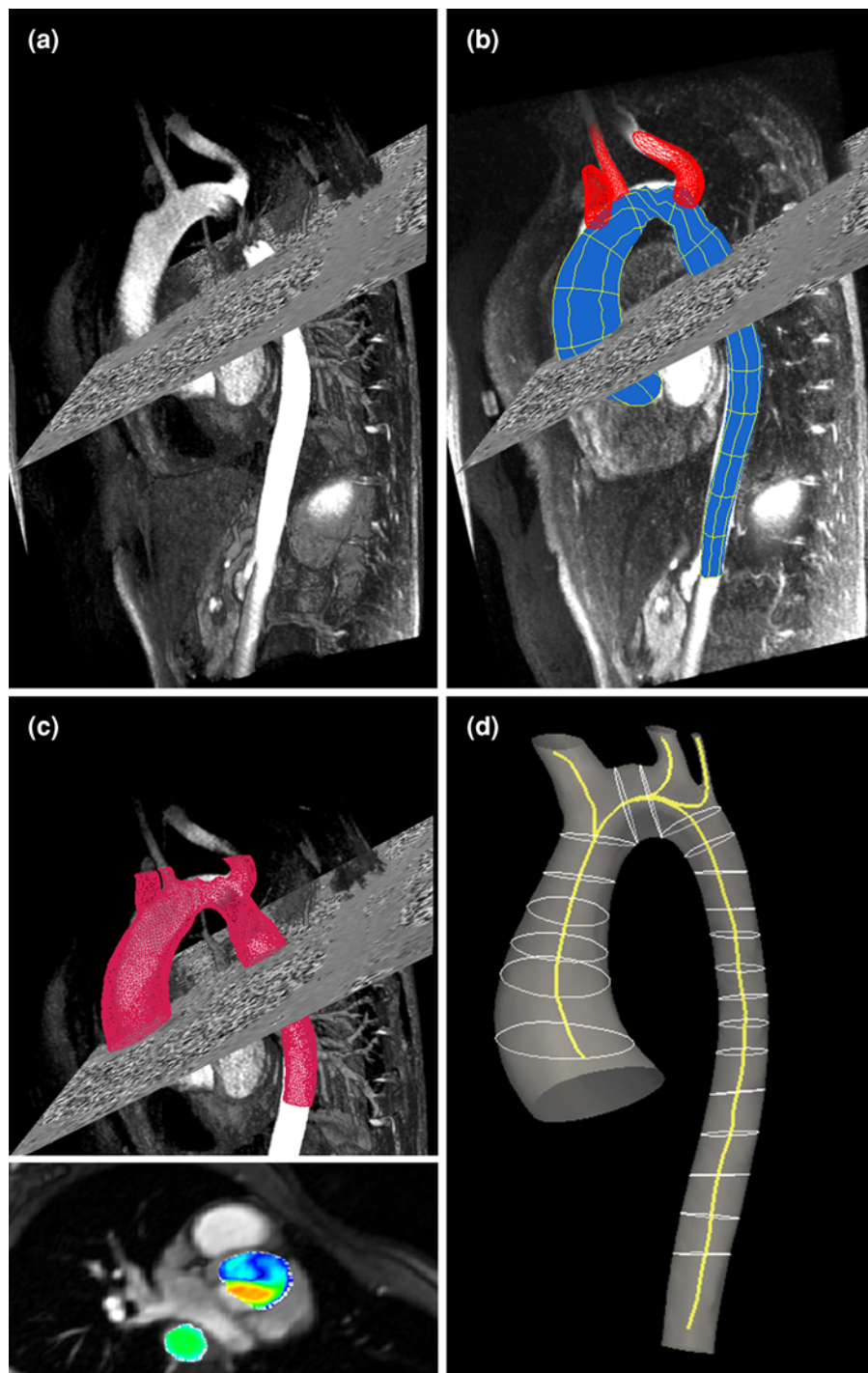


FIGURE 4. Pre-processing pipeline: (a) fusion of anatomic and flow MR images, (b) image segmentation: vessel wall extraction, (c) extraction of 3-D surface mesh and inflow flow profile, and (d) construction of 1-D model: centerline and cross-section extraction.

velocity before and after the coarctation were used to compute the trans-coarctation pressure-gradient by using the modified Bernoulli's equation.²⁰

Blood was modeled as an incompressible Newtonian fluid with a density of 1.055 g/cm^3 and a dynamic viscosity of $0.045 \text{ dynes/cm}^2 \text{ s}$ for all the computations.

A grid size of 0.05 cm was used leading to a computational model with 1200–1600 degrees of freedom (cross-sectional area and flow rate values) depending on the patient-specific geometry. Since an explicit numerical scheme has been adopted, the time step is limited by the CFL-condition, and has been set equal

TABLE 3. Patient data.

Patient no.	SBP (mmHg)	DBP (mmHg)	HR (bpm)	% Coarct. narrowing	\bar{Q}_{asc} (mL/s)	\bar{Q}_{desc} (mL/s)	Pressure gradients (mmHg)		
							Cath.	Doppler	Arm-leg
1	124	65	71	59.1	163.9	59.4	55	80	42
2	112	71	61	46.3	97.8	50.2	8	23	-3
3	124	71	118	47.9	88.6	61.5	30	67	40
4	89	50	74	39.5	199.5	85.7	14	27	27

TABLE 4. Comparison of average flow rate at the descending aorta and evaluation of coarctation resistance computation approaches.

Patient no.	PC-MRI (mL/s)	Flow computations (mL/s)	
		Using R_{c1}	Using R_{c2}
1	59.39	57.62	58.24
2	50.22	49.79	49.93
3	61.51	61.23	61.40
4	85.69	84.00	84.27
Mean rel. error (%)		1.56	1.09
Mean abs. error (mL/s)		1.04	0.74

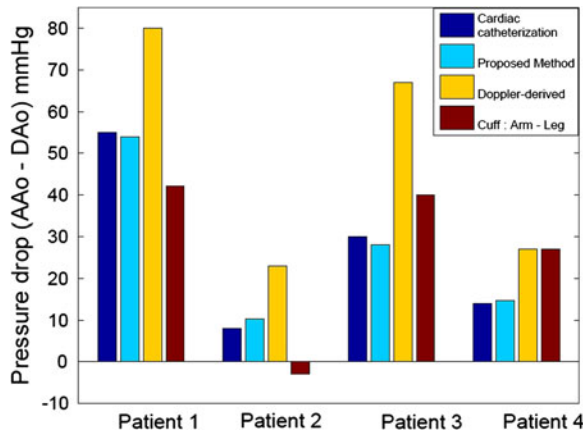


FIGURE 5. Comparison of pressure drops between ascending aorta and the descending aorta (AAo-DAo) at peak systole from four different methods—(i) invasive measurement from cardiac catheterization, (ii) proposed algorithm, (iii) Doppler echocardiography based measurement from modified Bernoulli’s equation, and (iv) cuff-pressure measurement in upper and lower body. For the proposed method, a mean absolute error of 1.45 mmHg was obtained for ΔP AAo-DAo, while the Doppler-derived and the cuff-pressure derived pressure gradients have an absolute error of 23 mmHg, and of 11.75 mmHg, respectively.

to 2.5×10^{-5} s. The first step has been to evaluate the two different approaches for the computation of the resistance introduced by the coarctation: R_{c1} and R_{c2} . Table 4 displays the average flow rate at the descending aorta, as determined through PC-MRI and as obtained by the reduced-order flow computations. In order to evaluate the approaches, we determined the mean relative error and the mean absolute error of the

computed average flow rate at the descending aorta. The relative error has been computed as $|Q_{measured} - Q_{computed}| / |Q_{measured}| \times 100$ and the absolute error as $|Q_{measured} - Q_{computed}|$. The results are displayed in the last two rows of Table 4 and show that, although the differences between the measured values and the computed ones are small for both approaches, the computed flow results are more accurate when R_{c2} is used. Hence, in the following, the resistance of the coarctation will be computed using the time-varying descending aorta flow rate.

Next, we compare the non-invasively computed trans-coarctation pressure gradient from our algorithm with (a) the clinical gold-standard measurements obtained during cardiac catheterization, (b) Doppler-echocardiography derived gradient using the modified Bernoulli’s equation, and (c) difference between the blood-pressure measurements in upper and lower body extremities; for the four patients. The pressure drops obtained with both our method and the catheter-based results were computed as peak-to-peak pressure drops between the ascending and the descending aorta. Figure 5 displays the results of the four-way comparison.

The results show an excellent agreement between the proposed algorithm and the invasive measurement, having a mean absolute error of 1.45 mmHg and a mean relative error of 10% for ΔP AAo-DAo. The Doppler-derived and the cuff-pressure derived pressure gradients have an absolute error of 23 mmHg, and of 11.75 mmHg, respectively, while the mean relative errors are of 112 and 72%, respectively.

TABLE 5. Comparison of pressure-drops and evaluation of pressure-drop models.

Patient no.	ΔP Cath. AAO-DAo (mmHg)	Pressure-drop computations AAO-DAo (mmHg)			
		Model in Eq. (12)	Model 1	Model 2	Model 3
1	55	53.97	58.33	40.67	41.41
2	8	10.28	11.00	5.49	5.82
3	30	28.11	29.46	19.81	20.34
4	14	14.62	15.40	7.56	8.16
Mean absolute error (mmHg)		1.45	2.07	8.36	8.18

DISCUSSION

The excellent validation results obtained for our non-invasive computation of trans-coarctation pressure-gradient demonstrate its feasibility for an accurate clinical assessment. The computation time ranged from 6 to 8 min, making it feasible for implementation in an existing clinical workflow. The discrepancy between the often used surrogate measures and the invasively measured trans-coarctation pressure-gradient further highlights the need for an accurate non-invasive assessment.

Our model personalization algorithm is applicable to not only quasi 1-D models, but can also be readily employed for 3-D CFD-based approaches. If the geometry model used for the computation is more detailed (i.e., has more branches), the methodology used for the computation of the outlet boundary condition does not change, the only difference is that the resistances/compliances are distributed among more terminal vessels. Furthermore, if the radiuses of the terminal vessels decrease, the distribution of the resistance values can be performed based on the assumption of a constant wall shear stress.⁷

The proposed methodology has been also tested using the three pressure drop models previously reported in literature and displayed in Table 1. The results are summarized in Table 5 for the four pressure-drop models, together with the invasive pressures obtained from cardiac catheterization.

To compare the performance of the pressure-drop models, we computed the mean absolute error of the pressure-drops between AAO-DAo and displayed it in the last row of the table. As can be seen, the model in Eq. (12) has the least error among the four models. From the four terms in the pressure-drop equation, the turbulent term has the highest contribution to the total pressure drop. Thus, the smaller values of K_t used in models 2 and 3 in Table 1 (0.95 and 1.0, respectively) are the main reason why the pressure drops obtained with these models are significantly smaller than the catheter-based values. By comparing the model in Eq. (12) and model 1, the differences are mainly given

by the fact that the inertial and viscous terms in Eq. (12) take into account the specific shape of the coarctation (the fourth term—continuous term—has a very small influence). We note however that the previously developed pressure-drop models, have neither been introduced specifically for coarctation narrowings, nor have they been used in a scenario similar to the herein described one, i.e., coupled to a full- or reduced-order CFD-based computational approach.

Since the trans-coarctation pressure gradient is computed as a peak-to-peak pressure difference between the ascending aorta and the descending aorta, the pressure drop is not mainly determined by the maximum flow rate and the geometry, but by the complex interaction between these two aspects, the phase lag introduced by the compliance,⁸ the wave propagation speed, and the backward travelling pressure and flow rate waves. Since the wave speed is determined individually for each patient, the proposed method is able to correctly model the arrival of reflected waves, which alter the flow rate waveform and potentially augment the peak pressure both in the ascending and descending aorta, thus influencing the final pressure-drop results. For the post-operative case, if a stent is placed, it will generally have different material properties than the aortic wall. This leads to an impedance mismatch at the two interfaces with the stent, and consequently to additional reflected waves at both interfaces, which impact the overall pressure and flow rate time-varying profiles. These aspects motivated our choice for using a one-dimensional wave-propagation based computational approach to capture the peak-to-peak trans-stenotic pressure drop.

In case of coarctation patients, significant collateral flow can appear around the coarctation. If the collateral vessels join the descending aorta at a location above the measurement point of the flow rate, then the computation of the coarctation resistance [Eqs. (13) and (14)] can no longer use the PC-MRI measured flow rate (since the flow rate through the coarctation would also contain the collateral flow, the pressure drop would be too high, and thus the coarctation resistance

would be overestimated). In this case a methodology based on the fact that the pressure drop between the aortic arch and the descending aorta has to be the same, regardless of the route which is followed (through the coarctation or through one of the collateral vessels), can be devised. Additionally, Eq. (13) should be used in this case, since it does not require the time-varying flow rate through the coarctation.

In case a stent is used during non-surgical catheter based repair, then the computation of the wave speed needs to be adapted. Since the material properties of the stent are known, the wave speed in the stented region can be determined (c_{stent}). Thus the wave speed of the rest of the aorta should be computed as follows:

$$c = \frac{\Delta x'}{\Delta t'} = \frac{\Delta x - \Delta x_{\text{stent}}}{\Delta t - \Delta x_{\text{stent}}/c_{\text{stent}}}, \quad (23)$$

whereas Δx and Δt are determined as before and Δx_{stent} is the length of the stented region.

In the following we compare our work with previously published methods and results.

Keshavarz-Motamed *et al.*¹⁰ have recently investigated the impact of concomitant aortic valve stenosis (AS) and coarctation on left ventricular workload, which is an important aspect since in 30–50% of CoA cases, AS is also present. A lumped parameter model was employed and showed that CoA has a smaller relative impact on LV workload (they showed that a severe CoA—90% area reduction—contributes less to the increase in LV work than a moderate AS—1.0 cm² effective orifice area). Further, they proposed a method to non-invasively estimate CoA severity from average flow through aortic valve and through CoA. Recently, two flow-rate independent measures of coarctation severity have been introduced,⁹ COA Doppler velocity index and COA effective orifice area, with promising results in an *in vitro* study. Together with the study reported herein, it enhances the possibilities of non-invasive evaluation of aortic coarctation.

Patient-specific 3-D rigid wall blood flow computations for a set of 5 patients have been reported earlier.²³ The inflow boundary condition was similar to the one in our proposed approach, flow rate conditions were applied directly at the supra-aortic vessels and a time-varying pressure waveform, as acquired through invasive catheter investigation, was applied at the descending aorta. The results are promising, but the method requires invasive measurements and thereby rendering it inadequate for a non-invasive estimation.

Coogan *et al.*³ examined the effects of stent-induced aortic stiffness on cardiac workload and blood pressure in post-intervention coarctation patients. A heart model was used as inlet boundary condition in order to

enable the simulation of conditions beyond those when the patient is imaged (e.g., exercise, post-treatment configurations). Since the goal of the present study was to provide an automatic personalization strategy for pre/post-operative cases, we have imposed directly the flow rate at the inlet.

LaDisa *et al.*¹¹ reported 3-D blood flow computations in pre- and post-operative coarctation patients. The PC-MRI acquired flow rate waveform at the ascending aorta was applied as the inflow boundary condition using a Poiseuille profile. The outlet boundary conditions of the supra-aortic vessels were determined by using the MAP and the PC-MRI acquired flow (the herein proposed methodology uses only ascending and descending aorta flow rate, the supra-aortic flow rates are estimated²⁸). The detailed procedure used for the descending aorta in the pre-operative cases though was not described and an iterative procedure is used in order to determine the wall properties. The work outlined detailed results regarding the time-averaged wall shear stress and oscillatory shear index, drawing significant conclusions based on the results obtained during both resting and exercise conditions. In the absence of invasive pressure measurements, the computed pressure drops were compared against the difference between the arms and legs pressure.

The methodology proposed herein introduces for all above mentioned papers complementary aspects, with a good potential of improving the results.

Our new method presented in this paper has important clinical implications:

- the personalization strategy for both pre- and post-operative data is fully automatic and requires no repetitive runs of the blood flow computation;
- reduced-order computations are usually more than two orders of magnitude faster than full-order models and can thus provide useful assistance for clinical decision making in a reasonable amount of time (in the order of minutes).

Our study has a series of limitations. Firstly, it has been tested only on four patients datasets thus far, and hence the results are preliminary and warrant a validation study on a larger number of datasets to be clinically relevant. Secondly, the proposed method (and its variant) has not been tested for geometries with significant collateral flow—case in which the proposed personalization strategy will need significant changes. Thirdly, the one-dimensional model introduces an approximation of the geometry, since an axisymmetric, tapering geometry is being considered. However, it has been shown that the one-dimensional model is able to predict time-varying pressure and flow

rate waveforms if the tapering is moderate,¹⁷ an assumption that might not hold for some geometries. Furthermore, though the direct imposition of flow-rate at the inlet of the aorta simplifies the personalization strategy both for the pre- and post-operative case, it makes the simulation of conditions beyond those at which the patient is imaged, impossible.

In terms of the pressure-drop model, it represents a semi-empirical approach which neglects the compliance of the coarctation region, i.e., the geometry of the coarctation is considered to be invariant in time for the computation of the pressure drop, and the parameter values used in Eq. (12) need to be validated in a study involving more patients.

CONCLUSIONS

In this paper, we presented a CFD-based approach coupled with a novel, non-invasive model personalization strategy for the non-invasive assessment of pre- and post-operative CoA patients.

We performed a validation study against *in vivo* clinical measurements obtained during routine cardiac catheterization, and obtained excellent agreement. The proposed approach is fully automatic, requiring no iterative tuning procedures, and a total of 6–8 min for the computation, being thus feasible in a clinical setting. We are in the process of expanding the validation study to more patients.

ACKNOWLEDGMENTS

The authors would like to acknowledge Dr. Michael Suehling and Dr. Constantin Suci. This work was partially supported by the Sectorial Operational Programme Human Resources Development (SOP HRD), financed from the European Social Fund and by the Romanian Government under the contract number POSDRU/88/1.5/S/76945. This work has been partially funded by European Union project Sim-e-Child (FP7 – 248421).

REFERENCES

- ¹Arzani, A., P. Dyverfeldt, T. Ebberts, and S. Shadden. In vivo validation of numerical prediction for turbulence intensity in an aortic coarctation. *Ann. Biomed. Eng.* 40:860–870, 2012.
- ²Bessems, D. On the Propagation of Pressure and Flow Waves Through the Patient-Specific Arterial System. PhD Thesis, TU Eindhoven, The Netherlands, 2007.
- ³Coogan, J. S., F. P. Chan, C. A. Taylor, and J. A. Feinstein. Computational fluid dynamic simulations of aortic coarctation comparing the effects of surgical- and stent-based treatments on aortic compliance and ventricular workload. *Catheter. Cardio. Interv.* 77:680–691, 2011.
- ⁴Formaggia, L., D. Lamponi, M. Tuveri, and A. Veneziani. Numerical modeling of 1D arterial networks coupled with a lumped parameters description of the heart. *Comput. Method. Biomech.* 9:273–288, 2006.
- ⁵Garcia, D., P. Pibarot, and L. G. Duranda. Analytical modeling of the instantaneous pressure gradient across the aortic valve. *J. Biomech.* 38:1303–1311, 2005.
- ⁶Hom, J. J., K. Ordovas, and G. P. Reddy. Velocity-encoded cine MR imaging in aortic coarctation: functional assessment of hemodynamic events. *Radiographics* 28:407–416, 2008.
- ⁷Ibrahim, E. S., K. Johnson, A. Miller, J. Shaffer, and R. White. Measuring aortic pulse wave velocity using high-field cardiovascular magnetic resonance: comparison of techniques. *J. Cardiovasc. Magn. Reson.* 12:26–38, 2010.
- ⁸Kadem, L., D. Garcia, L. G. Durand, R. Rieu, J. G. Dumesnil, and P. Pibarot. Value and limitations of peak-to-peak gradient for evaluation of aortic stenosis. *J. Heart Valve Dis.* 15:609–616, 2006.
- ⁹Keshavarz-Motamed, Z., J. Garcia, N. Maftoon, E. Bedard, P. Chetaille, and L. Kadem. A new approach for the evaluation of the severity of coarctation of the aorta using Doppler velocity index and effective orifice area: in vitro validation and clinical implications. *J. Biomech.* 45:1239–1245, 2012.
- ¹⁰Keshavarz-Motamed, Z., J. Garcia, P. Pibarot, E. Larose, and L. Kadem. Modeling the impact of concomitant aortic stenosis and coarctation of the aorta on left ventricular workload. *J. Biomech.* 44:2817–2825, 2011.
- ¹¹LaDisa, J. F. J., C. A. Figueroa, I. E. Vignon-Clementel, H. J. Kim, N. Xiao, L. M. Ellwein, F. P. Chan, J. A. Feinstein, and C. A. Taylor. Computational simulations for aortic coarctation: representative results from a sampling of patients. *J. Biomech. Eng.* 133:091008, 2011.
- ¹²Menon, A., D. C. Wendell, H. Wang, T. Eddinger, J. Toth, R. Dholakia, P. Larsen, E. Jensen, and J. F. J. LaDisa. A coupled experimental and computational approach to quantify deleterious, hemodynamics, vascular alterations, and mechanisms of long-term morbidity in response to aortic coarctation. *J. Pharmacol. Toxicol. Methods* 65:18–28, 2011.
- ¹³Mynard, J. P., and P. Nithiarasu. A 1D arterial blood flow model incorporating ventricular pressure, aortic valve and regional coronary flow using the locally conservative Galerkin (LCG) method. *Int. J. Numer. Method. Biomed. Eng.* 24:367–417, 2008.
- ¹⁴Olufsen, M., and C. Peskin. Numerical simulation and experimental validation of blood flow in arteries with structured-tree outflow conditions. *Ann. Biomed. Eng.* 28:1281–1299, 2000.
- ¹⁵Ralovich, K., L. Itu, V. Mihalef, P. Sharma, R. Ionasec, D. Vitanovski, W. Krawtschuk, A. Everett, R. Ringel, N. Navab, and D. Comaniciu. Hemodynamic assessment of pre- and post-operative aortic coarctation from MRI. Proceedings of MICCAI, Nice, France, October 2012.
- ¹⁶Razminia, M., A. Trivedi, J. Molnar, M. Elbzour, M. Guerrero, Y. Salem, A. Ahmed, S. Khosla, and D. L. Lubell. Validation of a new formula for mean arterial pressure calculation: the new formula is superior to the standard formula. *Catheter. Cardio. Interv.* 63:419–425, 2004.

- ¹⁷Reymond, P., Y. Bohraus, F. Perren, F. Lazeyras, and N. Stergiopoulos. Validation of a patient-specific one-dimensional model of the systemic arterial tree. *Am. J. Physiol. Heart C.* 301:1173–1182, 2011.
- ¹⁸Ringel, R. E., and K. Jenkins. Coarctation of the aorta stent trial (coast), 2007. <http://clinicaltrials.gov/ct2/show/NCT00552812>. Accessed March 10, 2012.
- ¹⁹Seeley, B. D., and D. F. Young. Effect of geometry on pressure losses across models of arterial stenoses. *J. Biomech.* 9:439–448, 1976.
- ²⁰Seifert, B. L., K. DesRochers, M. Ta, G. Giraud, M. Zarandi, M. Gharib, and D. J. Sahn. Accuracy of Doppler methods for estimating peak-to-peak and peak instantaneous gradients across coarctation of the aorta: an In vitro study. *J. Am. Soc. Echocardiogr.* 12:744–753, 1999.
- ²¹Steele, B. N., J. Wan, J. P. Ku, T. J. R. Hughes, and C. A. Taylor. In vivo validation of a one-dimensional finite-element method for predicting blood flow in cardiovascular bypass grafts. *IEEE Trans. Biomed. Eng.* 50:649–656, 2003.
- ²²Stergiopoulos, N., D. F. Young, and T. R. Rogge. Computer simulation of arterial flow with applications to arterial and aortic Stenoses. *J. Biomech.* 25:1477–1488, 1992.
- ²³Valverde, I., C. Staicu, H. Grotenhuis, A. Marzo, K. Rhode, Y. Shi, A. Brown, A. Tzifa, T. Hussain, G. Greil, P. Lawford, R. Razavi, R. Hose, and P. Beerbaum. Predicting hemodynamics in native and residual coarctation: preliminary results of a rigid-wall computational-fluid-dynamics model validated against clinically invasive pressure measures at rest and during pharmacological stress. *J. Cardiovasc. Magn. Reson.* 13:49, 2011.
- ²⁴Vignon-Clementel, I., C. A. Figueroa, K. Jansen, and C. A. Taylor. Outflow boundary conditions for 3D simulations of non-periodic blood flow and pressure fields in deformable arteries. *Comput. Methods Biomech. Biomed. Eng.* 13:625–640, 2010.
- ²⁵Vitanovski, D., K. Ralovich, R. Ionasec, Y. Zheng, M. Suehling, W. Krawtschuk, J. Hornegger, and D. Comaniciu. Personalized learning-based segmentation of thoracic aorta and main branches for diagnosis and treatment planning. 9th IEEE International Symposium on Biomedical Imaging, Barcelona, Spain, 2012.
- ²⁶Willett, N., R. Long, K. Maiellaro-Rafferty, R. Sutliff, R. Shafer, J. Oshinski, D. Giddens, R. Guldberg, and R. Taylor. An in vivo murine model of low-magnitude oscillatory wall shear stress to address the molecular mechanisms of mechanotransduction. *Arterioscler. Thromb. Vasc. Biol.* 30:2099–2102, 2010.
- ²⁷Young, D., and F. Tsai. Flow characteristics in models of arterial stenoses—II. Unsteady flow. *J. Biomech.* 6:547–559, 1973.
- ²⁸Zamir, M., P. Sinclair, and T. H. Wonnacott. Relation between diameter and flow in major branches of the arch of the aorta. *J. Biomech.* 25:1303–1310, 1992.